Songklanakarin J. Sci. Technol.
41 (1), 123-135, Jan. – Feb. 2019

http://www.sjst.psu.ac.th

Original Article

Stagnation point flow of thermally radiative and dissipative MHD nanofluid over a stretching sheet filled with porous medium and suction

R. V. M. S. S. Kiran Kumar* and S. Vijaya Kumar Varma

Department of Mathematics, Sri Venkateswara University,
Tirupati, Andhra Pradesh, 517502 India

Received: 11 July 2017; Revised: 5 September 2017; Accepted: 5 October 2017

Abstract

An analysis is carried out to examine the stagnation point flow of a nanofluid over a stretching surface through a porous medium in the presence of radiation and dissipation. The Buongiorno nanofluid model is incorporated in this study. The arising set of governing partial differential equations (PDE' s) of the flow is transformed into coupled non-linear ordinary differentials equations (ODE' s) with the help of appropriate similarity transformations and then solved numerically using boundary value problem default solver in MATLAB bvp4c package. To reveal the effects of the controlling parameters on the velocity, temperature, species concentration, the friction factor coefficient, the rate of heat and mass transfer coefficients are presented in graphical and tabular forms. It is found that the surface temperature in motivated with rising values of thermal radiation and thermophoresis parameters. From this we concluded that for heat enhancement processes thermal radiation and thermophoresis are very useful.

Keywords: MHD, porous medium**,** stagnation point flow, viscous dissipation, thermal radiation

1. Introduction

The point of which the local velocity of a fluid is zero is generally referred as stagnation - point flow. It has various practical applications in aerospace and aeronautical engineering such as a jet engine, heat controlling process and performance of solar thermal collectors etc. The study of stagnation-point flow was originated by Hiemenz (1911). The stagnation-point flow on stretching surface arises in plenty of practical applications in engineering as well as industry, for example cooling of nuclear reactors, electronic devices, polymer extrusion and drawing of plastic sheets etc. The analysis of stagnation-point flow over a stretching/ shrinking sheet with surface heat flux was studied by Suali, Nik Long, and Ishak (2012) . Generally, nanoparticles are made up of metal, metal oxide, carbide, and nitride and even immiscible nanoscale liquid droplets. The initial effort for the nanofluid was done by Choi (1995). Later Buongiorno (2006) presented convective transport in nanofluids and concluded that the thermal conductivity of nanofluids is very high compared to the base fluids. Khanafer, Vafai, and Lightstone (2003) studied the enhancement of heat transfer in a two-dimensional enclosure utilizing nanofluids. They developed a model to analyze the heat transfer performance of nanofluids in an enclosure taking into account the solid particle dispersion. Very recently, investigators (Gopinath, 2016; Khan *et al.* , 2016, 2017a, 2017b; Kiran Kumar, & Varma, 2017a, 2017b; Pal & Gopinath, 2017a, 2017b; Sheikholeslami, 2017a, 2017b) analyzed the mechanisms of thermophoresis and Brownian motion by considering the Buongiorno nanofluid model with different geometries. Also, researchers Sheikhole slami *et al.* (2017a, 2017b, 2017c, 2017d) studied the flow problems by taking different types of water - based nanoparticles.

The thought of stagnation-point flow of a nanofluid is comprehensive. Accordingly, Ishak, Jafar, Nazar, and Pop (2009) and Mahapatra and Gupta (2002) investigated the hydromagnetic stagnation-point flow over a stretching surface. Ibrahim, Shankar, and Nandeppanavar (2013) analysed the magnetic field effect on stagnation point flow in nanofluid

*Corresponding author
Email address: kksaisiva@gmail.com

near the stretching surface. Bachok, Ishak, and Pop (2011) examined stagnation point nanofluid flow over a stretching/ shrinking sheet by assuming the stretching/ shrinking velocity and the ambient fluid velocity change linearly with the distance from the stagnation point. Alsaedi, Awais and Hayat (2012) studied the influence of heat generation/ absorption on the stagnation-point nanofluid flow of over a linear stretching sheet. Mansur, Ishak, and Pop (2015) studied hydrodynamic stagnation point nanofluid flow over a permeable stretching/shrinking surface and found that raising the Brownian motion parameter and the thermophoresis parameter reduces the rate of heat transfer at the surface. Hady, Mohamed, and Ahmed (2014) analysed the stagnation - point nanofluid flow over a stretching sheet in the presence of magnetic field and porous media. Bachok, Ishak, and Pop (2012) examined the boundary layer stagnation-point flow of a water - based nanofluid past an exponentially stretching/ shrinking surface in its own plane. A theoretical investigation was carried out to scrutinize the effects of volume fraction of nanoparticles, suction/ injection, and convective heat and mass transfer effects on magneto-hydrodynamic stagnation - point flow of water-based nanofluids by Mabood, Pochai, and Shateyi, (2016). The mixed convection magnetohydrodynamic slip flow near a stagnation-point region over a non-linear stretching sheet with prescribed surface heat flux was illustrated by Shen, Wang, and Chen (2015).

The effects of variable fluid viscosity and thermal radiation on stagnation point flow over a stretching surface in a porous medium was reported by Mukhopadhyay (2013) and be concluded that the fluid temperature at a point of the surface is found to decrease with increasing thermal radiation. The flow of a Maxwell nanofluid with slip boundary conditions over a permeable stretching surface with radiation and dissipation has been considered by Nagendramma, Kiran Kumar, Durga Prasad, and Leelaratnam (2016). Mabood, Shateyi, and Rashidi (2016) analysed the hydromgnetic stagnation - point flow of a water - based nanofluid with radiation, dissipation and destructive chemical reaction effects. Magnetohydrodynamic effects on the convection flow of nanoparticles particles, namely, copper and alumina near a stagnation region past a vertical plate with viscous dissipation was examined by Mustafa, Javed, and Majeed (2015). Ul Haq, Nadeem, Khan, and Akbar (2015) considered the hydro-magnetic stagnation point flow of a radiative nanofluid passed over a stretching surface. Hafizi, Yasin, Ishak, and Pop (2015) studied the magnetohydrodynamic stagnation-point slip flow over a permeable stretching/shrinking sheet in the presence of dissipation and Joule heating.

Motivated by the above-mentioned works, the aim of the present study is to investigate the influence of viscous dissipation and thermal radiation on hydromagnetic stagnation-point flow of a nanofluid over a stretching sheet in a porous medium. The formulation of the problem is made through Buongiorno's model, which involves the aspects of Brownian motion and thermophoresis. The resulting set of governing equations has been solved numerically using MATLAB boundary value problem default solver bvp4c package. The results on velocity, temperature and nanoparticle concentration as well as the friction factor coefficient, the rate of heat and mass transfer coefficients are discussed and presented through graphs. Further, the results are compared

with exact solutions, which are reported by (Mahapatra, & Gupta, 2002).

2. Formulation of the Problem

We consider a steady laminar, viscous incom-pressible, two dimensional boundary layer stagnation-point flow of an electrically conducting nanofluid flow over a permeable stretching surface embedded in a porous medium coinciding with the plane $y = 0$ through fixed stagnation point at $x = 0$ as exposed in Figure 1. We assumed the Buongiorno's model, which involves the aspects of Brownian motion and thermophoresis. It is assumed that the surface temperature and nanoparticle concentration are T_w and C_w, respectively. $U_\infty(x) = bx$ is the free stream velocity and the plate is stretched with the velocity $u_w(x) = cx$, where b and c are positive constants. It is also assumed that v_0 is the constant mass flux with $v_0 > 0$ for injection and $v_0 < 0$ for suction. T_∞ and C_∞ are the ambient temperature and concentration, respectively. We choose the coordinate system such that the x-axis is along stretching sheet and the y-axis is perpendicular to the stretching sheet. The flow is subjected to constant magnetic field of strength $B = B_0$ which is assumed to be applied normal to the flow direction. It is assumed that the induced magnetic field is neglected due to small magnetic Reynolds. Also, the joule heating is neglected.

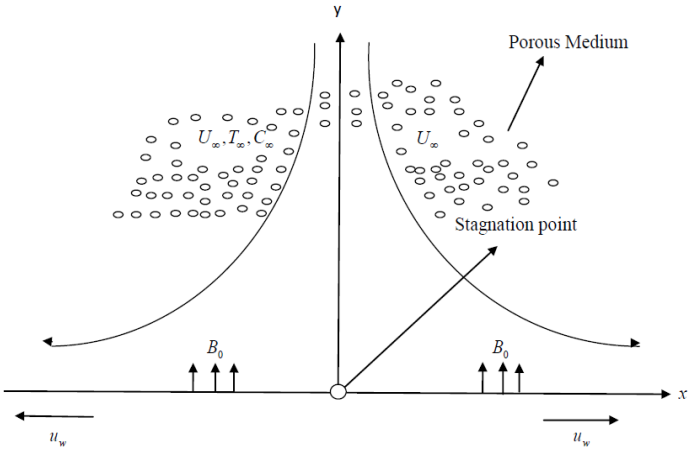

Figure 1. Physical model and co-ordinate system.

The basic equations for the steady flow of a nanofluid in the presence of magnetic field, porosity, viscous dissipation, thermal radiation, Brownian motion and thermophoresis are given by

$$\nabla \cdot V = 0 \tag{1}$$

$$\rho_f (V \cdot \nabla) V = -\nabla P + \mu \nabla^2 V + J \times B - \frac{\mu}{K_1} V \tag{2}$$

$$(\rho C_p)_f (V \cdot \nabla T) = k \nabla^2 T + (\rho C_p)_p \left(D_B \nabla C \nabla T + \left(\frac{D_T}{T_\infty} \right) \nabla T \nabla T \right) - \nabla q_r + \mu (\nabla V \nabla V) \tag{3}$$

$$(V\cdot\nabla C)=D_B\nabla^2 C+\left(\frac{D_T}{T_\infty}\right)\nabla^2 T \tag{4}$$

where $V=(u,v)$ is the nanofluid velocity vector, *P* is the pressure of the nanofluid, *B* is the magnetic induction intensity and *J* is the electrical current density.

Under the above assumptions the governing equations (1)-(4) take the following forms

$$\frac{\partial u}{\partial x}+\frac{\partial v}{\partial y}=0, \tag{5}$$

$$u\frac{\partial u}{\partial x}+v\frac{\partial v}{\partial y}=U_\infty\frac{dU_\infty}{dx}+v\frac{\partial^2 u}{\partial y^2}+\frac{\sigma B_0{}^2}{\rho_f}(U_\infty-u)+\frac{\mu}{\rho_f K_1}(U_\infty-u), \tag{6}$$

$$u\frac{\partial T}{\partial x}+v\frac{\partial T}{\partial y}=\alpha\frac{\partial^2 T}{\partial y^2}+\tau\left[D_B\frac{\partial C}{\partial y}\frac{\partial T}{\partial y}+\frac{D_T}{T_\infty}\left(\frac{\partial T}{\partial y}\right)^2\right]-\frac{1}{(\rho c_p)_f}\frac{\partial q_r}{\partial y}+\frac{\mu}{(\rho c_p)_f}\left(\frac{\partial u}{\partial y}\right)^2, \tag{7}$$

$$u\frac{\partial C}{\partial x}+v\frac{\partial C}{\partial y}=D_B\frac{\partial^2 C}{\partial y^2}+\frac{D_T}{T_\infty}\frac{\partial^2 T}{\partial y^2}, \tag{8}$$

Here u and v are the velocity components along x and y axes respectively. υ is the kinematic viscosity of the fluid, *T* is the temperature of the fluid, α is the thermal diffusivity, ρ_f is the density. ρc_p is the effective heat capacity of nanoparticle, ρ_f is the density of the base fluid, q_r is the radiative heat flux, $\tau=(\rho c)_p/(\rho c)_f$, is the proportion of effective heat capacity of the nanoparticle material to the effective heat capacity of the base fluid, c_f denotes specific heat of the fluid, and c_p denotes particle at constant pressure, respectively. D_B is the Brownian diffusion coefficient, D_T is the thermophoresis diffusion coefficient and *C* is the nanoparticle volume friction of.

Using Roseland approximations of radiation

$$q_r=-\frac{4\sigma^*}{3k^*}\frac{\partial T^4}{\partial y} \tag{9}$$

where k^* is the mean absorption coefficient, σ^* is Stephan Boltzman constant and T^4 is the linear temperature function and is expanded by using Taylor's series expansion in terms of T_∞ as

$$T^4=4T_\infty{}^3T-3T_\infty{}^4 \tag{10}$$

In view of Equations (9) and (10), the Equation (7) can be written as

$$u\frac{\partial T}{\partial x}+v\frac{\partial T}{\partial y}=\alpha\frac{\partial^2 T}{\partial y^2}+\tau\left[D_B\frac{\partial C}{\partial y}\frac{\partial T}{\partial y}+\frac{D_T}{T_\infty}\left(\frac{\partial T}{\partial y}\right)^2\right]+\frac{\mu_f}{(\rho c_p)_f}\left(\frac{\partial u}{\partial y}\right)^2+\frac{16\sigma^* T_\infty{}^3}{3(\rho c_p)_f k^*}\frac{\partial^2 T}{\partial y^2} \tag{11}$$

The appropriate boundary conditions are

$$t<0:\ u=v=0,\ T=T_\infty,\ C=C_\infty$$

$$t\geq 0: v=v_0,\ u=\lambda u_w(x)\ ,\ T=T_w,\ C=C_w \text{ at } y=0, \tag{12}$$

$$u\to U_\infty(x),\ T\to T_\infty,\ C\to C_\infty \text{ as } y\to\infty$$

Here $\lambda>0$ represents the stretching sheet and $\lambda<0$ for shrinking sheet.

3. Method of Solution

Introduce the following self-similarity variables as (Bachok *et al.* (2011))

$$\psi=\sqrt{cv}xf(\eta),\ \theta(\eta)=(T-T_\infty)/(T_w-T_\infty),\ \phi(\eta)=\frac{(C-C_\infty)}{(C_w-C_\infty)},\eta=\sqrt{c/\upsilon}y, \tag{13}$$

Let ψ be a stream function that satisfies the Equation (5) such that

$u=\partial\psi/\partial y$ and $v=-\partial\psi/\partial x$. Thus, we have

$$u=c\,x\,f'(\eta),\ v=-\sqrt{c\upsilon}\ f(\eta), \tag{14}$$

Using the above similarity variables in Equations (6)-(8), we get

$$f'''+ff''-f'^2+\left(M+\frac{1}{K}\right)(A-f')+A^2=0 \tag{15}$$

$$\frac{1}{\Pr}\left(1+\frac{4R}{3}\right)\theta''+f\theta'+Nt\,\theta'^2+Nb\theta'\phi'+Ecf''^2=0 \tag{16}$$

$$\phi''+Le\ f\phi'+\frac{Nt}{Nb}\theta''=0 \tag{17}$$

The associated dimensionless boundary conditions are given by

$$f(\eta)=S,\ f'(\eta)=\lambda,\ \theta(\eta)=1,\ \phi(\eta)=1,\ \text{at}\ \eta=0$$

$$f'(\eta)\to A,\ \theta(\eta)\to 0,\ \phi(\eta)\to 0\ \text{as}\ \eta\to\infty \tag{18}$$

where $S>0$ for suction and $S<0$ for injection, Pr is the Prandtl number, *M* is the magneticfield parameter, *K* is the porosity parameter is, *A* is the velocity ratio parameter , *Le* is the Lewis number is, *Nb* and *Nt* are the Brownian motion and thermophoresis parameters, respectively, *Ec* is the Eckert number and *R* is the thermal radiation parameter, defined as

$$\Pr=\frac{\upsilon}{\alpha}=\frac{\mu c_p}{k},\ Nb=\frac{\tau D_B(\phi_w-\phi_\infty)}{\upsilon},\ Nt=\frac{\tau D_T(T_w-T_\infty)}{\upsilon T_\infty},\ Le=\frac{\upsilon}{D_B},$$

$$S=-\frac{v_0}{\sqrt{a\upsilon}},\ M=\frac{\sigma B_0^{\,2}}{\rho_f c},\ A=\frac{b}{c},\ Ec=\frac{u_w^{\,2}}{c_p(T_w-T_\infty)},\ R=\frac{4\sigma^* T_\infty^{\,3}}{kk^*},\ K=\frac{c\rho_f K_1}{\mu_f} \tag{19}$$

The physical quantities of interest are the friction factor coefficient (C_f), and the local Nusselt number (Nu_x), and the reduced Sherwood number (Sh_x), and are defined as

$$C_f = \frac{\tau_w}{\rho u_w^{\,2}(x)},\ Nu_x = \frac{xq_w}{k(T_w - T_\infty)},\ Sh_x = \frac{xq_m}{D_B(C_w - C_\infty)} \tag{20}$$

where τ_w is the skin friction along the plate and q_w is the heat flux from the plate, which are defined as

$$\tau_w = \mu\left(\frac{\partial u}{\partial y}\right)_{y=0},\ q_w = -k\left(\frac{\partial T}{\partial y}\right)_{y=0},\ q_m = -D_B\left(\frac{\partial C}{\partial y}\right)_{y=0} \tag{21}$$

In view of Equation (13), we get

$$\mathrm{Re}_x^{1/2} C_f = f''(0),\ \mathrm{Re}_x^{-1/2} Nu_x = -\theta'(0),\ Sh_x = -\mathrm{Re}_x^{1/2}\phi'(0) \tag{22}$$

The local Reynolds number is defined as $\mathrm{Re}_x = u_w(x)\,x/\upsilon$.

4. Numerical Procedure

In this section, we present a numerical procedure of the above boundary value problem. In general, a boundary value problem (BVP) consists of a set of ordinary differential equations (ODE's), some boundary conditions, and guesses that depend on which solution is desired.

The procedure for the present problem is

$$f''' = -\left(ff'' - f'^2 + \left(M + \frac{1}{K}\right)(A - f') + A^2\right),$$

$$\theta'' = -\mathrm{Pr}\Big/\left(1 + \frac{4R}{3}\right)\left(f\theta' + Nt\,\theta'^2 + Nb\theta'\phi' + Ecf''^2\right),$$

$$\phi'' = -\left(Le\, f\phi' + \frac{Nt}{Nb}\theta''\right).$$

Subject to the boundary conditions $f(0) = S$, $f'(0) = \lambda, \theta(0) = 1, \phi(0) = 1$, $f'(0) = A$, $\theta(0) = 0$, $\phi(0) = 0$.

We can choose the guess in the following form (Ascher, Mattheij, Russell, 1995)

$$u(x) = \lambda u_w(x),$$

$$v(x) = v_0,$$

$$T(x) = T_w(x),$$

$$C(x) = C_w(x),$$

$$u(x) = U_\infty(x)$$

$$T(x) = T_\infty(x),$$

$C(x) = C_\infty(x)$.

To solve this problem with bvp4c in Matlab, we provide functions that evaluate the differential equations and the residual in the boundary conditions. These functions must return column vectors with components of f corresponding to the original variables as

$f(1) = f$, $f(2) = f'$, $f(3) = f''$, $f(4) = \theta$, $f(5) = \theta'$, $f(6) = \phi$ and $f(7) = \phi'$. These functions can be coded in MATLAB as

```
function dydx = exlode(x,f)
dydx = [-((f(1)*f(3))-(f(2)^2)+((M+1/K)*(A-f(2)))+A^2)
-((Pr/(1+(4*R/3)))*((f(1)*f(5))+(Nt*f(5)^2)+(Nb*f(5)*f(7))+(Ec*(f(3)^2))))
-((Le*f(1)*f(7))+(Nt/Nb)*(-((Pr/(1+(4*R/3)))*((f(1)*f(5))+
(Nt*f(5)^2)+(Nb*f(5)*f(7))+(Ec*(f(3)^2))))))];
function res = exlbc(fa,fb)
res = [fa(1)-S
    fa(2)-λ
    fa(4)-1
    fa(6)-1
    fb(2)-A
    fb(4)
    fb(6)];
```

The guess is supplied to bvp4c in the form of a structure. Whereas the name *solinit* will be used in this problem, we can call it anything we like. But, it must contain two fields that must be called *x* and *f*. A guess for a mesh that reveals the behaviour of the solution is provided as the vector *solinit.x*. A guess for the solution at these mesh points is provided as the array *solinit.y*, with each column *solinit.f (:, i)* approximating the solution at the point *solinit.x(i)*. It is not difficult to form a guess structure, but a helper function *bvpinit* makes it easy in the most common circumstances. It creates the structure when given the mesh and a guess for the solution in the form of a constant vector or the name of a function for evaluating the guess.

The guess structure is then developed with *bvpint* by

```
solinit = bvpinit(linspace(0, 1, infinity), @exlinit);
```

The boundary value problem has now been defined by means of functions for evaluating the differential equations and the boundary conditions and a structure providing a guess for the solution. When default values are used, that is all needed to solve the problem with bvp4c:

```
sol = bvp4c(@shootode,@shootbc,solinit);
```

The output of bvp4c is a structure called here sol. The mesh determined by the code is returned as *sol.x* and the numerical solution approximated at these mesh points is returned as *f=sol.y.* As with the guess, *sol.f* (:, i) approximates the solution at the point *sol.x(i).*

5. Results and Discussion

The obtained coupled non-linear ordinary differential Equations (ODE's) (15)-(17) with corresponding boundary conditions (18) are numerically solved using bvp4c with Matlab package. The above mentioned numerical method is carried out for different values of flow factors to discuss the effects on velocity, temperature and nanoparticle concentration fields. The obtained results are shown in Figures 2–12. The friction factor coefficient the Nusselt number and Sherwood number are derived and presented in tabular form. Table1 shows the correctness of the method used and verified with the prevailing results and they are found to be very good agreement with Mahapatra and Gupta (2002). In the calculations the parametric values are selected as $Nb = 0.1$, $R = 0.1, Pr = 1, \mathrm{K} = 0.5, S = 0.5, A = 0.2, Nt = 0.1, Le = 1,$ $\lambda = 0.5, M = 1, Ec = 0.2$.

Figure 2 shows the influence of suction/injection parameter (S) on $f'(\eta)$. It is evident that the thickness of the momentum boundary layer decreases as *S* increases. This happens due to this fact that applying suction leads to draw the amount of fluid particles into the wall and subsequently the velocity boundary layer decreases. The effect of magnetic field parameter (*M*) on $f'(\eta)$ is exposed in Figure 3. It can be seen that the existence of magnetic field sets in a resistive force called Lorentz force, which is a retarding force on the velocity field; consequently, the velocity is reduced. Figure 4 depicts the variation of nanoparticle concentration profiles for various values of Brownian motion parameter (*Nb)*. It is noticed that as *Nb* increases, the thickness of the nanoparticle concentration boundary layer is decreased. Furthermore, the boundary layer thickness decreases in the liquid film with increasing values of *Nb*. Figure 5 illustrates the influence of thermophoresis parameter *(Nt)* on $\theta(\eta)$. It is clear that as the thermophoresis affect increases, a movement of nanoparticles from the hot surface to cold ambient fluid occurs, and thus the temperature of the fluid increases within the thermal boundary layer. This results in the development of thermal boundary layer thickness.

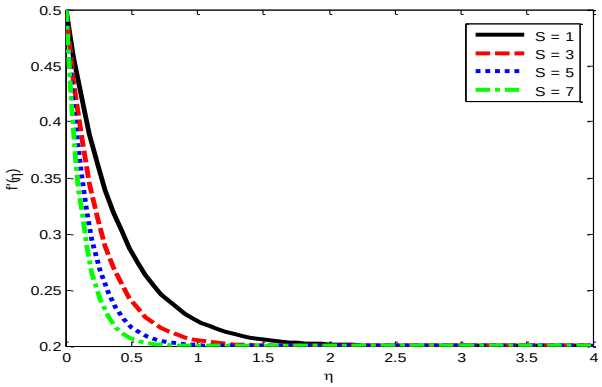

Figure 2. Velocity profiles for various values of *S*.

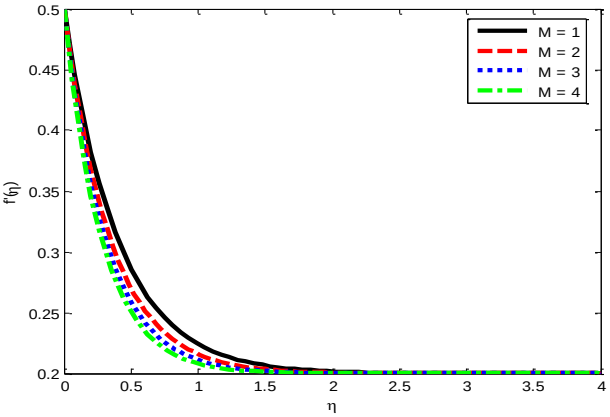

Figure 3. Velocity profiles for various values of *M*.

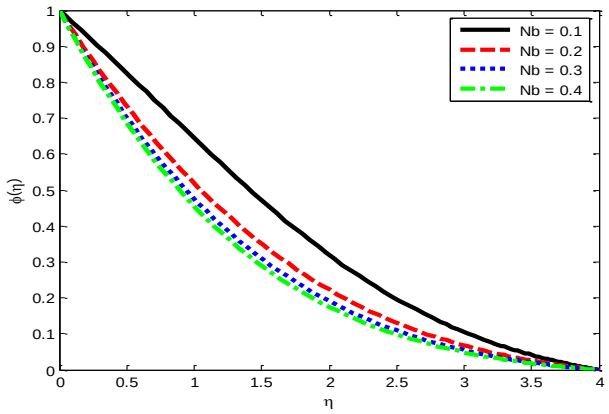

Figure 4. Concentration profiles for various values of *Nb*.

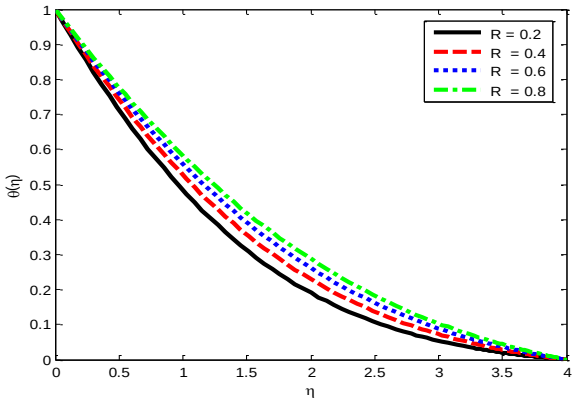

Figure 6. Temparature profiles for various values of *R*.

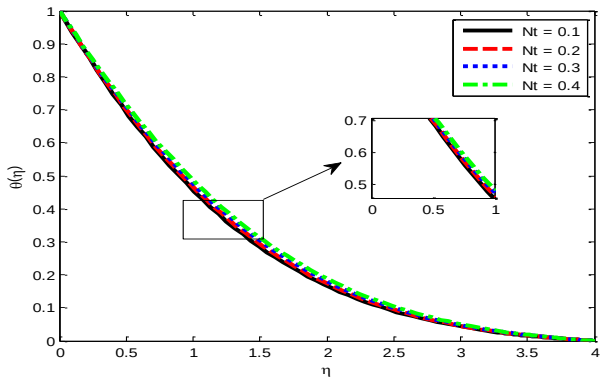

Figure 5. Temparature profiles for various values of *Nt*.

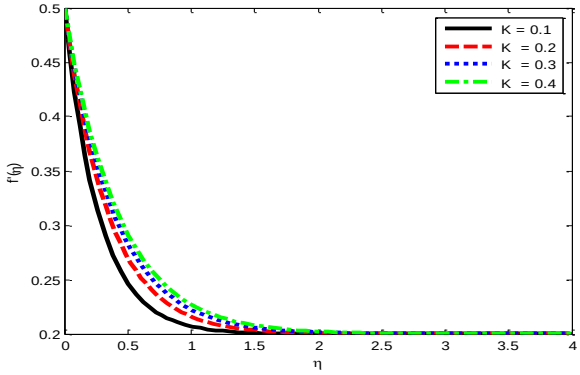

Figure 7. Velocity profiles for various values of *K*.

The effect of radiation parameter (*R*) on $\theta(\eta)$ is shown in Figure 6. It can be observed that increasing the values of *R* enhances the fluid temperature. Physically, increasing the values of *R* corresponds to an increased dominance of conduction over absorption radiation, thus increasing the temperature profiles. Also, increasing *R* produces a significant increase in the thermal boundary layer. In fact, the radiation parameter decreases the fluid temperature. This is because as the radiation parameter increases, the mean Rosseland absorption co-efficient *k** decreases. Hence, the thermal radiation factor is better suitable for cooling process. The effect of permeability of the porous medium parameter (*K*) on fluid velocity field is shown in Figure 7. As *K* increases the fluid velocity increases along the boundary layer, which is expected since when the holes of porous medium become larger, the resistivity of the medium may be abandoned and hence thickness of the hydromagnetic boundary layer increases. Figures 8 and 9 display the graphical representation of velocity and temperature distributions for different values of velocity ratio parameter (*A*). From Figure 8, it is seen that the free stream velocity exceeds the stretching surface velocity; the flow velocity increases the momentum boundary layer thickness and decreases with increase in *A*. Moreover, when the free stream velocity is less than the stretching velocity, the flow field velocity decreases and the boundary layer thickness also decreases. When $A > 1$, the flow has a boundary layer structure and thickness of the boundary layer decreases as

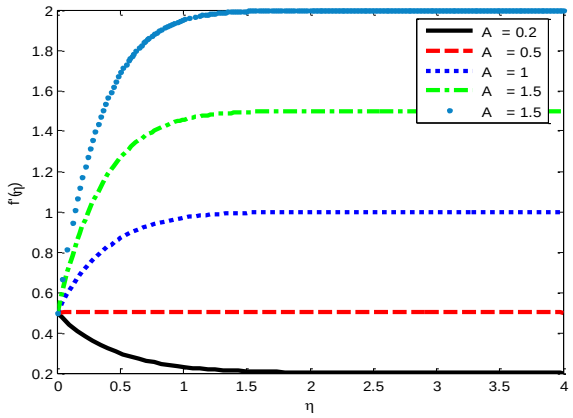

Figure 8. Velocity profiles for various values of *A*.

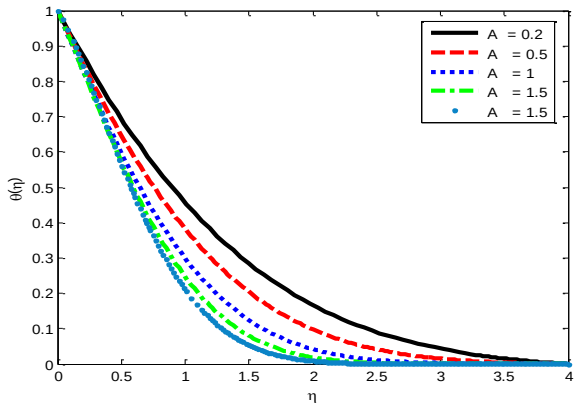

Figure 9. Temparature profiles for various values of *A*.

increase in *A*. Further, for $A<1$, the flow has a reversed boundary layer structure, for this case also we observe the depreciation in the boundary layer thickness. But the opposite phenomenon is noticed on temperature profiles (Figure 9).

The impact of stretching/shrinking parameter (λ) on $f'(\eta)$ is plotted in Figure 10. It is clear that when λ increases, then the velocity distribution diminishes. Physically, this phenomena can be described for various fixed values of stretching sheet; an increment in λ depicts an increment in straining motion near to the stagnation region, which suggests an increment on external stream and this tends to lead the thinning of boundary layer. The opposite trend is observed for shrinking parameter $(\lambda>0)$, that is, it reduces

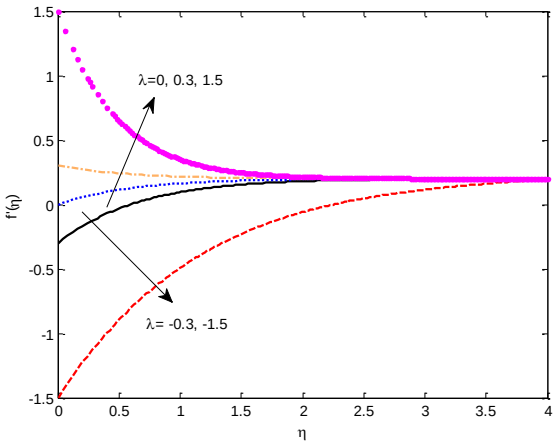

Figure 10. Velocity profiles for various values of λ .

the hydromagnetic boundary layer thickness. Further, we conclude that the changes occurring for a shrinking sheet $(\lambda>0)$ are more pronounced than those of a stretching sheet $(\lambda>0)$.

Figure 11 presents the temperature profiles for various values of Eckert number (Ec). Physically, Ec is the ratio of the kinetic energy of the flow to the boundary layer enthalpy difference. The influence of Ec on flow field is to enhance the energy, yielding a better fluid temperature. For this reason, the temperature increases. Also, higher viscous dissipative heat causes a rise in the thermal boundary layer. Figure 12 illustrates the graphical comparison of the present results with the results of (Mahapatra & Gupta, 2002).

Tables 1 and 2 present the numerical values of the friction factor coefficient $f''(0)$ and reduced local Nusselt number $-\theta'(0)$ for different values of *A* and Pr in the case of $M=0$, $K\to\infty$, $R=0$ and $Ec=0$, $S=0$, $Nt=0$, $Nb=0$, $\lambda=1$. The results are in good agreement with the existing result in Mahapatra and Gupta (2002).

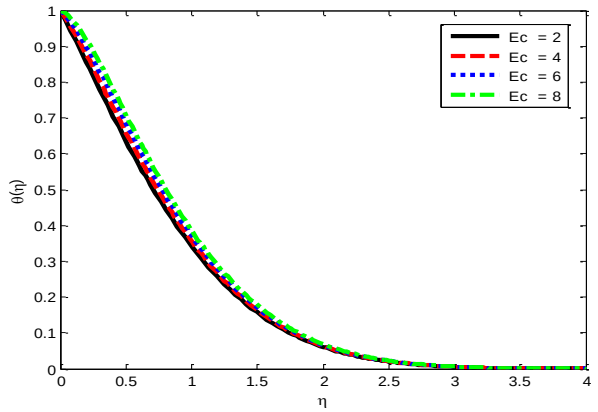

Figure 11. Temparature profiles for various values of *Ec*.

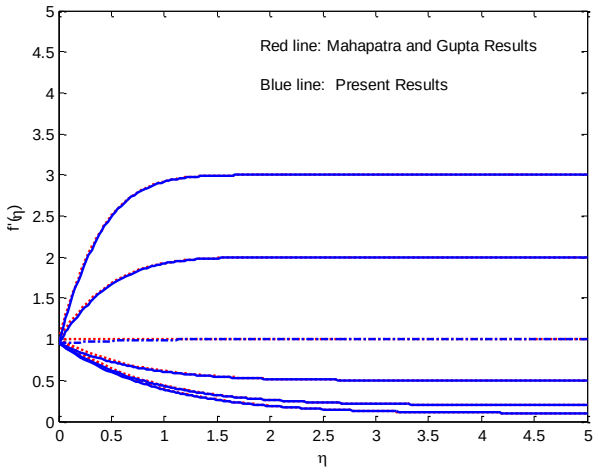

Figure 12. Graphical comparison of the present study with (Maha patra & Gupta, 2002).

Table 1. Comparison of skin-friction coefficient $f''(0)$ for different values of *A*.

A	(Mahapatra & Gupta, 2002)	Present Study
0.01	-	-0.998404
0.1	-0.9694	-0.969436
0.2	-0.9181	-0.918113
0.5	-0.6673	-0.667264
2	2.0175	2.017503
3	4.7293	4.729282

Table 2. Comparison of local Nusselt number $-\theta'(0)$, for different values of Pr and *A*.

Pr	A	(Mahapatra & Gupta, 2002)	Present Study
1	0.1	0.603	0.602158
1	0.2	0.625	0.624469
1	0.5	0.692	0.692449
1.5	0.1	0.777	0.776801
1.5	0.2	0.797	0.797122
1.5	0.5	0.863	0.864794

From Table 3, we found that an increase in *M* boosts the skin friction coefficient. As expected, the skin friction increases as the magnetic field strength values increase. Physically, the purpose of a magnetic field perpendicular to the fluid flow produces a drag force which tends to retard the fluid flow velocity, thus increasing the skin friction coefficient. But the reverse trend is observed on Nusselt number and Sherwood number. Then again the skin friction decreases with an increase in porosity parameter, but no effect of *R* and *Ec* on skin friction coefficient is seen. The Nusselt number increases with an increase in *K*, whereas it decreases with an increase in *M*, *R* and *Ec*. Finally, it is found that the rate of mass transfer coefficient increases with the increasing values of *K*, *R* and *Ec*, but the opposite trend is observed with an increase in *M*.

Table 3. Numerical values of skin friction coefficient, Nusselt number and Sherwood number for various values of M, R, K and Ec with $\Pr = 1, S = 0.2, Nt = Nb = 0.1, \lambda = 0.5, A = 0.2, Le = 0.5$.

M	*R*	*K*	*Ec*	$f''(0)$	$-\theta'(0)$	$-\phi'(0)$
1.0	0.5	0.5	0.1	0.616179	0.471543	0.278771
2.0				0.688410	0.464857	0.278537
3.0				0.753486	0.459383	0.278578
0.5	0.2			0.576514	0.451579	0.299848
	0.4			0.576514	0.404045	0.342304
	0.6			0.576514	0.369481	0.373523
		0.1		1.039083	0.364164	0.349250
		0.2		0.783926	0.374010	0.352971
		0.3		0.676929	0.379397	0.355614
			0.2	0.576514	0.380592	0.363729
			0.4	0.576514	0.370798	0.373153

6. Concluding Remarks

The effect of viscous dissipation and thermal radiation on hydromagnetic stagnation point flow of a nanofluid through porous medium over a stretching surface with suction is investigated. The obtained similarity ordinary

differential equations (ODE's) are solved by using Matlab bvp4c package. Based on the present study, the following conclusions are made.

1. The skin friction coefficient on the wall surface decreases with rising values of porosity parameter.
2. The heat transfer rate at the surface depreciated for higher values of radiation parameter and Eckert number.
3. The magnitude of mass transfer coefficient increases with radiation parameter and Eckert number.
4. The velocity profiles are suppressed by increasing values of suction.
5. An increase in velocity ratio parameter enhances the velocity boundary layer thickness.
6. The thermal radiation and thermophoresis parameters effectively enhance the surface temperature.

Acknowledgements

The authors wish to express their thanks to the reviewers for their very good comments and suggestions.

References

Alsaedi, A., Awais, M., & Hayat, T. (2012). Effects of heat generation/ absorption on stagnation point flow of nanofluid over a surface with convective boundary conditions. *Communications in Nonlinear Science and Numerical Simulation, 17*, 4210–4223.

Ascher, U., Mattheij, R., & Russell, R. (1995). *Numerical solution of boundary value problems for ordinary differential equations*. Philadelphia, PA: SIAM.

Bachok, N., Ishak, A., & Pop, I. (2011). Stagnation-point flow over a stretching/ shrinking sheet in a nanofluid. *Nanoscale Research Letters, 6*, 1-10.

Bachok, N., Ishak, A., & Pop, I. (2012). Boundary layer stagnation-point flow and heat transfer over an exponentially stretching/ shrinking sheet in a nanofluid. *International Journal of Heat and Mass Transfer, 55*, 8122–8128.

Buongiorno, J. (2006). Convective transport in nanofluids. *ASME Journal of Heat Transfer, 128*, 240-250.

Choi, S. U. S. (1995). Enhancing thermal conductivity of fluids with nanoparticles developments applications of non-Newtonian flows. D. A. Signine and H. P. Wang, ASME, New York, 66, 99-105.

Gopinath, M. (2016). Convective-radiative heat transfer of micropolar nanofluid over a vertical non-linear stretching sheet. *Journal of Nanofluids, 5*, 852-860.

Hiemenz, K. (1911). Die Grenzschicht an einem in den gleichförmigen Flüssigkeitsstrom eingetauchten geraden Kreiszylinder. *Dingler' s Polytech Journal, 326*, 321-410.

Hady, F. M., Mohamed, R. E., & Ahmed, M. (2014). Slip effects on unsteady MHD stagnation point flow of a nanofluid over stretching sheet in a porous medium with thermal radiation. *Journal of Pure and Applied Mathematics: Advances and Applications, 12*, 181-206.

Hafizi, M., Yasin, Mat., Ishak, A., & Pop, I. (2015). MHD stagnation-point flow and heat transfer with effects of viscous dissipation, joule heating and partial velocity slip. *Scientific Reports, 5*, 1-8.

Ishak, A., Jafar, K., Nazar, R., & Pop, I. (2009). MHD stagnation point flow towards a stretching sheet. *Physica A*: *Statistical Mechanics and its Applications, 388*, 3377–3383.

Ibrahim, W., Shankar, B., & Nandeppanavar, M. M. (2013). MHD stagnation point flow and heat transfer due to nanofluid towards a stretching sheet. *International Journal of Heat and Mass Transfer, 56*, 1–9.

Khan, M., & Azam, M. (2017a). Unsteady heat and mass transfer mechanisms in MHD Carreau nanofluid flow. *Journal of Molecular Liquids, 225*, 554–562.

Khan, M., Azam, M., & Alshomrani, A. S. (2017b). On unsteady heat and mass transfer in Carreau nanofluid flow over expanding or contracting cylinder. *Journal of Molecular Liquids, 231*, 474–484.

Khan, M., & Azam, M. (2016). Unsteady boundary layer flow of Carreau fluid over a permeable stretching surface. *Results in Physics, 6*, 1168-1174.

Khanafer, K., Vafai, K., & Lightstone, M. (2003). Buoyancy-driven heat transfer enhancement in a two-dimensional enclosure utilizing nanofluids. *International Journal of Heat and Mass Transfer, 46*, 3639-3653.

Kiran Kumar, R. V. M. S. S., & Varma, S. V. K. (2017a). Hydromagnetic boundary layer slip flow of nanofluid through porous medium over a slendering stretching sheet. *Journal of Nanofluids, 6*, 852-861.

Kiran Kumar, R. V. M. S. S., & Varma, S. V. K. (2017b). Multiple slips and thermal radiation effects on MHD boundary layer flow of a nanofluid through porous medium over a nonlinear permeable sheet with heat source and chemical reaction. *Journal of Nanofluids, 6*, 48-58.

Mahapatra, T. R., & Gupta, A. G. (2002). Heat transfer in stagnation point flow towards a stretching sheet. *Heat and Mass Transfer, 38*, 517–521.

Mansur, S., Ishak, A., & Pop, I. (2015). The Magnetohydrodynamic stagnation point flow of a Nanofluid over a stretching/shrinking sheet with suction. *PLOS ONE, 10*, 1-14.

Mabood, F., Pochai, N., & Shateyi, S. (2016). Stagnation point flow of nanofluid over a moving plate with convective boundary condition and magnetohydrodynamics. *Journal of Engineering, 2016*, 1-11.

Mukhopadhyay, S. (2013). Effects of thermal radiation and variable fluid viscosity on stagnation point flow past a porous stretching sheet. *Meccanica, 48*, 1717–1730.

Mabood, F., Shateyi, S., Rashidi, M. M., Momoniate, E., & Freidoonimehr, N. (2016). MHD stagnation point flow heat and mass transfer of nanofluids in porous medium with radiation, viscous dissipation and chemical reaction. *Advanced Powder Technology, 27*, 742–749.

Mustafa, I., Javed, T., & Majeed, A. (2015). Magnetohydrodynamic (MHD) mixed convection stagnation point flow of a nanofluid over a vertical plate with viscous dissipation. *Canadian Journal of Physics, 93*, 1365-1374.

Nagendramma, V., Kiran Kumar, R. V. M. S. S., Durga Prasad, P., Leelaratnam, A., & Varma, S. V. K. (2016). Multiple slips and radiation effects on Maxwell nanofluid flow over a permeable stretching surface with dissipation. *Journal of Nanofluids, 5*, 817-825.

Pal, D., & Gopinath, M. (2017a). Thermal radiation and MHD effects on boundary layer flow of micropolar nanofluid past a stretching sheet with non-uniform heat source/ sink. *International Journal of Mechanical Sciences, 126*, 308-318.

Pal, D. , & Gopinath, M. (2017b). Double diffusive magnetohydrodynamic heat and mass transfer of nanofluids over a nonlinear stretching/ shrinking sheet with viscous-Ohmic dissipation and thermal radiation. *Propulsion and Power Research, 6*, 58-69.

Rizwan, U. H., Nadeem, S., Khan, Z. H., & Akbar, N. S. (2015). Thermal radiation and slip effects on MHD stagnation point flow of nanofluid over a stretching sheet. *Physica E, 65*, 17–23.

Suali, M., Nik Long, N. M. A., & Ishak, A. (2012). Unsteady stagnation point flow and heat transfer over a stretching/ shrinking sheet with prescribed surface heat flux. *Applied Mathematics and Computational Intelligence, 1*, 1-11.

Sheikholeslami, M. (2017a). Numerical simulation of magnetic nanofluid natural convection in porous media. *Physics Letters A, 381*, 494–503.

Sheikholeslami, M. (2017b). Influence of Lorentz forces on nanofluid flow in a porous cylinder considering Darcy model. *Journal of Molecular Liquids, 225*, 903–912.

Sheikholeslami, M., & Seyednezhad, M. (2017a). Nanofluid heat transfer in a permeable enclosure in presence of variable magnetic field by means of CVFEM. *International Journal of Heat and Mass Transfer, 114*, 1169–1180.

Sheikholeslami, M., & Shehzad, S. A. (2017b). Thermal radiation of ferrofluid in existence of Lorentz forces considering variable viscosity**.** *International Journal of Heat and Mass Transfer, 109*, 82–92.

Sheikholeslami, M., & Shamlooei, M. (2017c). Fe_3O_4-H_2O nanofluid natural convection in presence of thermal radiation. *International Journal of Hydrogen Energy, 42*, 5708–5718.

Sheikholeslami, M. , Hayat, T. , & Alsaedi, A. (2017d) . Numerical study for external magnetic source influence on water based nanofluid convective heat transfer. *International Journal of Heat and Mass Transfer, 106*, 745–755.

Shen, M. , Wang, F. , & Chen, H. (2015) . MHD mixed convection slip flow near a stagnation-point on a nonlinearly vertical stretching sheet. *Boundary Value Problems, 78*, 1-15.